

# PREPARATION, CHARACTERIZATION AND OSTEOREGENIC POTENTIAL OF AN INJECTABLE PHOTO-CURABLE HYALURONIC ACID HYDROGEL SCAFFOLD LOADED WITH BIOACTIVE NANO-HYDROXYAPATITE

Mohamed M. Abdul-Monem<sup>1\*</sup> *MSc*, Fayza H. Al-Abbassy<sup>2</sup> *PhD*, Hanaa M. Aly<sup>3</sup> *PhD*, Dawlat M. Ahmed<sup>4,5</sup> *PhD*, Elbadawy A. Kamoun<sup>6,7</sup> *PhD*, Esmail M. El-Fakharany<sup>8</sup> *PhD*.

## ABSTRACT

**INTRODUCTION:** In-situ photo-cured hydrogels for bone regeneration offer an advantage compared to solid scaffolds or membranes is that it can be used by minimally invasive techniques and can fill irregularly shaped defects easily.

**OBJECTIVE:** was to prepare an injectable photo-curable hyaluronic acid hydrogel scaffold loaded with bioactive nano-hydroxyapatite using riboflavin as a natural source photoinitiator for bone regeneration and to investigate the effect of addition of nano-hydroxyapatite on the physiochemical and mechanical properties of the prepared hydrogel. Also, the osteogenic potential of the prepared hydrogels was assessed in a rabbit model.

**MATERIALS AND METHODS:** Two groups were prepared, (Group I) photo-cured hyaluronic acid as a control group and (Group II) photo-cured hyaluronic acid/nano-hydroxyapatite. Laboratory characterization tests: FTIR, XRD, SEM, mechanical, swelling and degradation rate tests were performed. Cell viability % using the MTT assay was used to assess the biocompatibility. In vivo bioactivity was assessed in a rabbit model and histomorphometric analysis was done.

**RESULTS:** Statistical analysis of results revealed that the addition of nano-hydroxyapatite increased significantly the mechanical properties of the hydrogels. SEM images demonstrated that the addition of nano-hydroxyapatite caused the formation of inter-connected pores. MTT assay showed that hydrogel extract didn't affect cell viability after 48h. Histomorphometric analysis results revealed that the photo-cured (GMA-HA/HAP) hydrogel increased the osteogenic potential by one and a half folds compared to the control group and this proved its bioactivity.

**CONCLUSION:** Results suggest that the prepared photo-cured hyaluronic hydrogel is a promising biomaterial to deliver bioactive nano-hydroxyapatite and has an osteogenic potential.

**KEYWORDS:** Hyaluronic acid, Visible-light, Riboflavin, Bone regeneration, Hydrogel.

<sup>1</sup> Assistant lecturer, Dental Biomaterials Department, Faculty of Dentistry, Alexandria University, Alexandria, Egypt.

<sup>2</sup> Professor, Dental Biomaterials Department, Faculty of Dentistry, Alexandria University, Alexandria, Egypt.

<sup>3</sup> Professor, Oral Biology Department, Faculty of Dentistry, Alexandria University, Alexandria, Egypt.

<sup>4</sup> Assist. Professor, Dental Biomaterials Department, Faculty of Dentistry, Alexandria University, Alexandria, Egypt.

<sup>5</sup> College of Dentistry, The Arab Academy for Science and Technology and Maritime Transport, El-Alamein, Egypt.

<sup>6</sup> Associate Professor, Polymeric Materials Research Department, City of Scientific Research and Technological Applications, Alexandria, Egypt.

<sup>7</sup> Nanotechnology Research Center, The British University in Egypt, Cairo, Egypt.

<sup>8</sup> Associate Professor, Protein Research Dep., Genetic Engineering and Biotechnology Research Institute, City of Scientific Research and Technological Applications, Alexandria, Egypt.

\*Corresponding author:

E-mail: [mohamed.mahmoud@dent.alex.edu.eg](mailto:mohamed.mahmoud@dent.alex.edu.eg)

## INTRODUCTION

Traditional methods for repairing bone defects include autografts, allografts, and xenografts, which despite being used widely, had several disadvantages that limited their clinical applications. Autografts offer a limited supply with multiple postoperative complications while allografts and xenografts have an increased risk of disease transmission and host rejection (1).

Synthetic bone scaffolds (alloplasts) are increasingly being used in bone regeneration applications to overcome the disadvantages of the previous types. Different alloplasts such as polymers, metals, ceramics and composites can be used for bone regeneration. Injectable

hydrogels; a type of alloplasts, are hydrophilic networks of cross-linked polymers that offer an advantage compared to solid scaffolds or membranes is that they can be used by minimally invasive techniques and have the ability to fill irregular bone faults (2). In-situ visible light photo-curing has become one of the attractive techniques to prepare injectable hydrogels for bone regeneration applications.

Hyaluronic acid is a negatively charged hydrophilic polysaccharide, made of D-glucuronic acid and N-acetyl-D-glucosamine which acts as an essential constituent of the extracellular matrix (3). For hyaluronic acid to be photo-cured, the addition of a methacrylate group with (C=C) is achieved by reacting with glycidyl methacrylate.

Modification of hyaluronic acid is mandatory to improve its low mechanical properties and fast rate of degradation to promote its applicability (4). This can be done by adding fillers such as silanized nano-hydroxyapatite. Nano-Hydroxyapatite is a bioactive element essentially required for bone regeneration by osteoconduction or by serving as a scaffold for filling bony faults. Hydroxyapatite surface allows osteoblastic cell adhesion, growth, and differentiation thus new bone is formed by the creeping substitution from surrounding bone (5).

Riboflavin or vitamin B2, is found in the human body, it is biocompatible and absorbs light in the range of 330 - 470 nm, thus it can act as a natural alternative to synthetic photoinitiators. Riboflavin has the ability to produce superoxide radicals which can consequently initiate a polymerization reaction (6). The null hypothesis to be tested is that the addition of nano-hydroxyapatite to photo-cured hyaluronic acid hydrogels will have no effect on the physiochemical, mechanical and osteogenic properties.

## MATERIALS AND METHODS

### Materials

Hyaluronic acid (HA) ( $M_w = 10,000\text{--}15,000$  g/mol) was obtained from (Shanghai Jiaoyuan Industry, Shanghai, China). Glycidyl methacrylate (GMA), 3-Aminopropyltriethoxysilane (APTES), riboflavin 5'-monophosphate sodium salt hydrate (RF), triethyl amine (TEA), diphenyliodonium chloride (DPIC), nano-hydroxyapatite (HAP) (size  $<200$  nm) and Van Gieson's stain were purchased from (Sigma Aldrich, Missouri, USA). Tetrabutyl ammonium bromide (TBAB) was purchased from (MP Biomedicals, Eschwege, Germany). 2-Dimethylaminoethyl methacrylate (DMAEMA) was obtained from (Acros organics, New Jersey, USA). Acetone was purchased from (Tedia, Ohio, USA). RPMI 1640 medium was purchased from (Lonza, Maryland, USA). MTT was purchased from (Thermo Fisher scientific, Massachusetts, USA). Methyl methacrylate and Stevenel's blue stain were purchased from (Loba chemie Ltd., India).

### Methods

#### *1. Preparation of glycidyl methacrylate-hyaluronic acid (GMA-HA) copolymer*

To prepare methacrylated hyaluronic acid copolymer (GMA-HA) to be used to prepare photo-curable hydrogels, 1g hyaluronic acid (HA) dissolved in 60 ml water was reacted with 3ml glycidyl methacrylate (GMA) in the presence of 3 ml triethyl amine as a catalyst and 3g tertbutyl ammonium bromide as a phase transfer catalyst under magnetic stirring at  $70^\circ\text{C}$  for 2 hours (7, 8). After cooling to room temperature, the mixture was precipitated in acetone then the GMA-HA precipitate was freeze-dried and stored at  $4^\circ\text{C}$  for preparation of hydrogel groups.

To confirm the methacrylation of hyaluronic acid, proton nuclear magnetic resonance ( $^1\text{H-NMR}$ ) spectroscopy was used. The NMR spectrum was recorded at 300 Hz using a  $^1\text{H-NMR}$  device (NMR-DRX400, Brucker, Germany) by dissolving 50 mg of (GMA-HA) copolymer in 1 ml of deuterium oxide (9).

#### *2. Silanization of nano-hydroxyapatite surface*

Nano-hydroxyapatite (HAP) surface was chemically modified before addition to the (GMA-HA) polymer solution to ensure homogenous distribution and adequate

bond with the hyaluronic acid hydrogel matrix. First, 5 wt.% aminopropyl triethoxysilane (APTES) was added to 50 ml ethyl alcohol (90%) and heated at  $70^\circ\text{C}$  for one hour. Then, 3g nano-hydroxyapatite ( $< 200$  nm) was added and further mixed for one hour, followed by ultra-sonication for 30 minutes. The mixture was then centrifuged, and the precipitate was washed twice with water to eliminate free unreacted APTES, then dried in an oven overnight at  $70^\circ\text{C}$  (10).

#### *3. Preparation of photo-cured hyaluronic acid hydrogel groups*

To prepare group I hydrogel, GMA-HA copolymer (12.5 %, wt./v) was dissolved in 4 ml distilled water and photo-cured by LED lamp (2000 mW/cm $^2$ , Denjoy DY 400, Shanghai, China) utilizing a photoinitiating system, composed of (1 wt. % ) riboflavin 5'-monophosphate sodium salt hydrate (RF) as a photoinitiator, (0.025 %, v/v) dimethylaminoethyl methacrylate (DMAEMA) as a coinitiator, and (0.5 wt.%) diphenyl iodonium chloride (DPIC) as an accelerator (Table 1). The mixture was kept under stirring for 30 minutes in a brown glass vial to avoid premature polymerization from the surrounding light. To prepare hydrogel discs for laboratory characterization, the mixture was injected into polytetrafluoroethylene molds and photo-cured by LED lamp at zero distance irradiation exposure (Figure 1).

For preparation of group II hydrogel, (0.5 mg/ml) of silanized nano-hydroxyapatite (Table 1) was added to the polymer-photoinitiating system, stirred for 30 min. and then ultra-sonicated for 15 min. to ensure homogenous distribution and then photo-cured by LED lamp (Figure 1).

#### *4. Laboratory characterization of photo-cured hydrogel scaffolds*

##### *a) Fourier-transform infrared spectroscopy (FTIR)*

FTIR spectra of silanized nano-hydroxyapatite powder, uncured (GMA-HA) copolymer powder and photo-cured hydrogels lyophilized powder of the two groups, were recorded by (Shimadzu FTIR-8400S, Kyoto, Japan). Transparent discs were prepared by mixing the powder to be tested with potassium bromide (KBr) and then pressing into discs .The FTIR spectra were recorded between 4000 and 400 cm $^{-1}$ (11). The degree of conversion (DC %) of the two groups was calculated from FTIR spectra based on the ratio of GMA conjugated (C=C) transmittance peak area ( $\nu \sim 1535$  cm $^{-1}$ ) to carbonyl ester group peak area ( $\nu \sim 1710$  cm $^{-1}$ ) as a reference before and after curing of the specimens (11, 12), according to the following equation:

$$\text{DC \%} = 1 - \left( \frac{(1535 \text{ cm}^{-1}/1710 \text{ cm}^{-1}) \text{ peak area after curing}}{(1535 \text{ cm}^{-1}/1710 \text{ cm}^{-1}) \text{ peak area before curing}} \right) \times 100.$$

##### *b) X-ray diffraction (XRD)*

XRD patterns of silanized nano-hydroxyapatite and lyophilized hydrogel powder of the two groups were obtained using an x-ray diffractometer (Shimadzu XRD-6100, Kyoto, Japan) using copper K-alpha energy. The patterns were recorded in between ( $10^\circ\text{--}70^\circ$ ) at a speed of 5 min $^{-1}$  (13).

##### *c) Surface morphology*

The surface morphology of lyophilized hydrogel discs was examined by a scanning electron microscope (SEM), (JEOL, JSM-6360LA, Tokyo, Japan). Hydrogel discs were immersed in distilled water for 24 h to swell and then lyophilized at (-90 °C). The lyophilized hydrogel discs were

then gold coated using an ion sputter coater and examined (11). Transmission electron microscope (TEM), (JEM 2100, JEOL, Tokyo, Japan) was used to ensure homogenous distribution of silanized nano-hydroxyapatite after ultrasonic dispersion of modified powder into ethanol (14).

*d) Mechanical properties*

A rheometer (HAAKE MARS III, Thermo-Fisher Scientific, Massachusetts, USA) was used to measure the mechanical properties of the photo-cured hydrogels. The polymer-photoinitiating mixture for each of the two groups ( $n=5$ ) was photo-cured in-situ the measuring plate, forming photo-cured hydrogel discs (5mm thick and 25mm in diameter) and the storage modulus ( $G'$ ) was measured by measuring the oscillatory shear and rotational flows at 25°C with a frequency sweep ranging from 0.1 to 10 Hz (15).

*e) Measurement of equilibrium swelling*

For each group, hydrogel discs ( $n=5$ ) were placed in distilled water and weighed daily to determine increasing weight and volume due to swelling. Repetition of this step was done till no change in the hydrogel discs' weight was found and the discs reached the equilibrium swelling state. The discs were freeze-dried and the water uptake (%) was determined as follows (16):

$$\text{Water uptake (\%)} = \frac{W_s - W_0}{W_0} \times 100$$

Where,  $W_s$  is the weight of swollen hydrogel disc and  $W_0$  is the weight of freeze-dried hydrogel disc.

*f) Rate of degradation*

For each group, hydrogel discs ( $n=5$ ) were placed in phosphate buffer solution ( $\text{pH}=7.4$ ) at 37°C and the solution was changed daily. After 28 days, hydrogel discs were taken from the PBS, washed with distilled water to remove salts and then lyophilized. The percentage weight loss (%WL) of hydrogel discs was calculated using the following equation:

$$\%WL = ((W_i - W_f)/W_i) \times 100$$

Where,  $W_i$  is the initial dry weight of hydrogel disc and  $W_f$  is the weight of the dry hydrogel disc after placement in phosphate buffer solution. Then the remaining weight % was calculated by subtracting (% WL) from 100% (17).

*g) Cell viability (%)*

Effect of swollen hydrogel extract on cell viability % human peripheral blood mononuclear cells (PBMCs) was determined using dimethylthiazole diphenyltetrazolium bromide (MTT) assay, which is a colorimetric assay for measuring cell metabolic activity. PBMCs cells ( $1.0 \times 10^3$ ) were seeded into 96-well sterile flat bottom tissue culture micro-plates and cultured in RPMI-1640 media, supplied with 10% fetal bovine serum and incubated at 37°C in 5% CO<sub>2</sub> for one day. 50 µl of swollen hydrogel extract from each group was added to the cells and incubated for 48 hours. After incubation, the hydrogel extract was removed, and the cells were washed thrice with PBS to remove debris and non-viable cells. 200 µl of MTT solution was added per well and incubated for 5 h. Purple Formazan crystals were then dissolved in 200 µl/well of dimethyl sulfoxide (DMSO) and the absorbance (A) was measured at 630 nm using an ELISA microplate reader. The cell viability (%) was calculated using the following equation, where (A) is the absorbance and the control are wells containing cells without hydrogel extract (18, 19):

$$\text{Cell viability \%} = (A_{\text{test}} / A_{\text{control}}) \times 100$$

*5. In vivo bioactivity assessment and histomorphometric analysis*

Bioactivity of the prepared hydrogels was assessed in vivo in a femoral defect in a rabbit model. Six New Zealand white rabbits were used as test subjects, three rabbits per group. Surgical procedures were performed according to the guidelines set out by the Ethics Research Committee of the Faculty of Dentistry, Alexandria University (IRB No.: 00010556-IORG 0008839). For each group, autoclave sterilized (5 minutes at 118°C) hydrogels (20) were injected into a surgical defect (4 mm in diameter and 5 mm in depth) in the right and left femur of each rabbit and photo-cured in-situ for 10 seconds.

After six weeks, rabbits were euthanized, and the right and left femur of each rabbit were obtained. Femur heads were fixed in 10% buffered formalin, then dehydrated in ascending concentrations of ethyl alcohol from (70-100%), followed by clearing in xylene and finally embedding in methyl methacrylate. 100 µm thick undecalcified sections were obtained using a precision cutter and stained using Van Gieson's and Stevenel's blue stains (21). Histomorphometric analysis was done using ImageJ software (National institute of health, USA), to calculate new bone area % in a region of interest (ROI), according to the following equation (22):

$$\text{New bone area \%} = \frac{\text{New trabeculae area}}{\text{ROI area}}$$

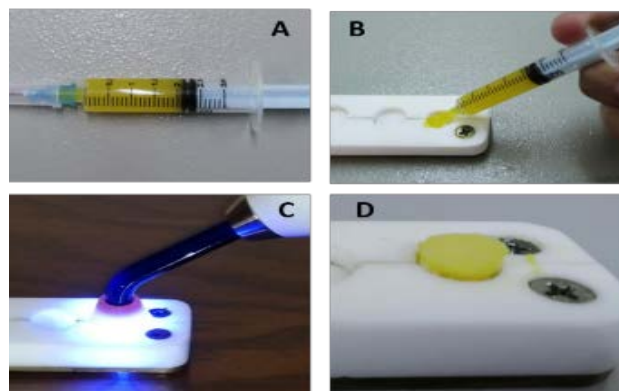
*Statistical analysis*

Statistical analysis of data was done using Tukey's post-hoc test for comparison between the two groups, at a significance level of 0.05. Analysis of data was done by (IBM SPSS version 20.0).

**Table 1:** Composition of the photo-cured hydrogel groups.

Group	Photo-cured Hydrogel	Copolymer (wt/v %)	HAP (mg/ml)	Riboflavin Photoinitiator (wt%)	DMAEMA Coinitiator (v/v%)	DPIC Accelerator (wt %)
I	GMA-HA	12.5 %	-	1	0.025	0.5
II	GMA-HA/HAP	12.5 %	0.5	1	0.025	0.5

**Figure 1:** (A) Injectable photo-cured hyaluronic acid hydrogel (B) Injecting hydrogel into mold (C) Photo-curing using LED lamp for 10 seconds (D) Photo-cured hydrogel disc.



## RESULTS

Methacrylation of hyaluronic acid (GMA-HA) was verified by the appearance of methacrylate protons of GMA and methyl group of hyaluronic acid at in the  $^1\text{H-NMR}$  spectrum and the degree of methacryylation was calculated to be (~36 %). FTIR spectra of APTES modified nano-hydroxyapatite is shown in (Figure 2A). Two peaks of phosphate functional groups ( $\text{PO}_4^{3-}$ ) were detected at wavelengths ( $\nu \sim 1030$  and  $603 \text{ cm}^{-1}$ ). Other peaks shown at ( $\nu \sim 3440 \text{ cm}^{-1}$ ) and at ( $\nu \sim 1640 \text{ cm}^{-1}$ ) corresponded to the stretching and bending modes of the hydroxyl group (OH), respectively. Presence of Si-O at ( $\nu \sim 850 \text{ cm}^{-1}$ ), Si-O-Si at ( $\nu \sim 1100 \text{ cm}^{-1}$ ), C-H at ( $\nu \sim 1460 \text{ cm}^{-1}$ ), N-H at ( $\nu \sim 3200 \text{ cm}^{-1}$ ) and Si-OH at ( $\nu \sim 3436 \text{ cm}^{-1}$ ) all confirmed surface modification of nano-hydroxyapatite by APTES.

FTIR spectrum of un-cured (GMA-HA) (Figure 2B) showed the appearance of a band at ( $\nu \sim 3450 \text{ cm}^{-1}$ ) which is attributed to (OH and NH) stretching regions of hyaluronic acid. The bands at ( $\nu \sim 1631$ , 1402, and  $1068 \text{ cm}^{-1}$ ) correspond to the amide carbonyl group ( $\text{NC=O}$ ), carboxylic group ( $\text{COO}$ ) and hydroxyl group (OH) of hyaluronic acid, respectively. The spectrum also shows the appearance of transmission bands of conjugated aliphatic ( $\text{C=C}$ ) of GMA at ( $\nu \sim 1535 \text{ cm}^{-1}$ ). In group I and II, photo-curing led to the breakdown of ( $\text{C=C}$ ) and a decrease in the intensity of transmission bands at ( $\nu \sim 1535 \text{ cm}^{-1}$ ) (Figure 2C and 2D). Degree of conversion was calculated to be ( $92.30 \pm 0.67$ ) % for group I and ( $51.0 \pm 1.0$ ) % for group II with a statistically significant difference (Table 2). In both groups, hydrogel discs (8 mm in diameter and 5 mm in height formed after 10 seconds of irradiation with LED lamp.

XRD patterns of modified nano-hydroxyapatite (Figure 3A) showed the appearance of hydroxyapatite characteristic peaks at  $2\Theta$  ( $31.77^\circ$ ,  $32.19^\circ$  and  $32.90^\circ$ ). The pattern of group I (Figure 3B) shows the amorphous nature of hyaluronic acid while the pattern of group II (Figure 3C) shows the semi-crystalline nature due to addition of crystalline nano-hydroxyapatite to amorphous hyaluronic acid with hydroxyapatite characteristic peaks. SEM images revealed that, the surface morphology of group I photo-cured hydrogel (Figure 4A) seems to be compacted, dense and somewhat regular. However, the addition of hydroxyapatite to group II (Figure 4B) led to the formation of interconnected polyhedral pores that mimic bone trabecular structure. The average pore size diameter was calculated to be (~ $100 \mu\text{m}$ ). TEM images revealed the homogenous distribution of silanized nano-hydroxyapatite with no agglomeration, further confirming the successful surface modification of nano-hydroxyapatite (Figure 5).

The addition of nano-hydroxyapatite to group II showed a 2-fold increase in the storage modulus ( $7.56 \pm 0.34$ ) KPa, than in group I ( $3.48 \pm 0.36$ ) KPa with a statistically significant difference (Table 2). The equilibrium swelling state for the both groups was reached after 5 days, regardless the hydrogel composition. Group I showed less water uptake ( $97.04 \pm 0.11$ ) % with a significant difference compared to group

II ( $98.46 \pm 0.18$ ) % (Table 2). The remaining weight % of group I and II was ( $51.0 \pm 1.0$ ) % and ( $51.30 \pm 0.84$ ) % respectively. There was no significant difference in the degradation rate after 28 days between the two groups. MTT assay of PMBCs showed that the prepared hydrogels were biocompatible after incubation of cells in hydrogel extract after 48 hours. The cell viability % of group I was ( $75.60 \pm 0.27$ ) %, which was higher than that of group II ( $73.50 \pm 0.27$ ) % with a statistically significant difference (Table 2).

In vivo bioactivity assessment of the prepared hydrogels revealed that group II increased the osteogenic potential by one and a half folds ( $43.63 \pm 4.55\%$ ), compared to the control group ( $26.76 \pm 2.52$ ), (Table 2). Microscopic pictures revealed that in group II, lamellar bone trabeculae formed by creeping substitution from the original bone, filling the center of the defect (Figure 6C). In group I, few bone islands were formed in the periphery of the surgical defect (Figure 6A). The osteocytes formed in group II (Figure 6D), were smaller in size and more organized than in the control group I (Figure 6B).

**Table 2:** ANOVA using Tukey's post hoc test to compare between groups.

Groups	Group I: GMA-IIA	Group II: GMA-IIA/HAP
Degree of conversion	( $92.30 \pm 0.67$ ) <sup>a</sup>	( $51.0 \pm 1.0$ ) <sup>b</sup>
Water uptake %	( $97.04 \pm 0.11$ ) <sup>a</sup>	( $98.46 \pm 0.18$ ) <sup>b</sup>
Remaining wt. % after 28 days	( $51.0 \pm 1.0$ ) <sup>a</sup>	( $51.30 \pm 0.84$ ) <sup>a</sup>
Storage modulus ( $\text{G}'$ ) (KPa)	( $3.48 \pm 0.36$ ) <sup>a</sup>	( $7.56 \pm 0.34$ ) <sup>b</sup>
Cell Viability %	( $75.60 \pm 0.27$ ) <sup>a</sup>	( $73.50 \pm 0.27$ ) <sup>b</sup>

a,b indicate significant difference between groups ( $p < 0.05$ )

**Figure 2:**  $^1\text{H-NMR}$  spectrum of GMA-HA copolymer where, (a,b,c) are methacrylate protons of GMA and (d) is methyl proton of hyaluronic acid.

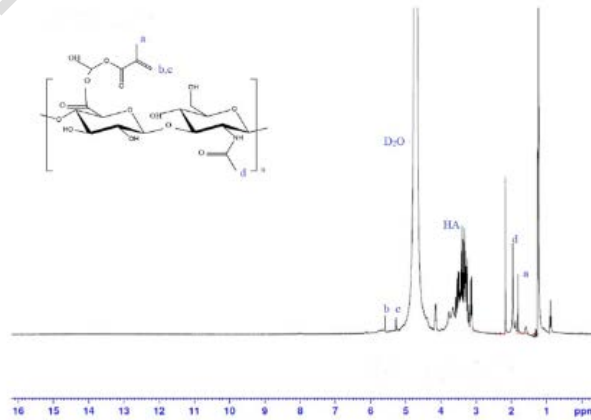


**Figure 3:** FTIR spectra: (A) Silanized nano-hydroxyapatite (B) Un-cured GMA-HA copolymer (C) Photo-cured GMA-HA (group I) (D) Photo-cured GMA-HA/HAP (group II)

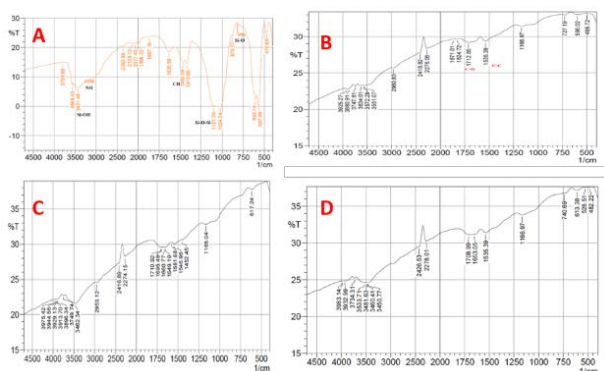


**Figure 4:** XRD patterns (A) Silanized nano-hydroxyapatite ,(B) Photo-cured GMA-HA (group I),(C) Photo-cured GMA-HA/HAP (group II).Arrows showing characteristic peak of nano-hydroxyapatite at 32° .

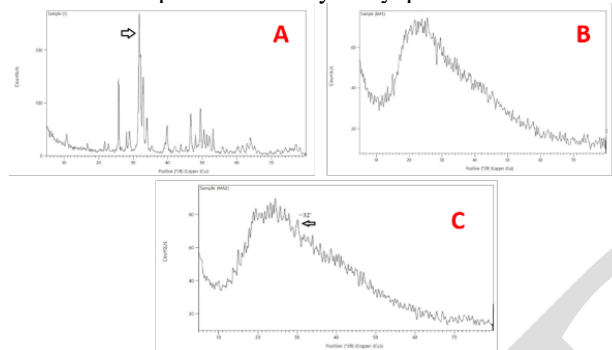


**Figure 5:** SEM images (A) Photo-cured GMA-HA (group I), showing dense compact surface, (B) Photo-cured GMA-HA/HAP (group II) , showing porous structure .

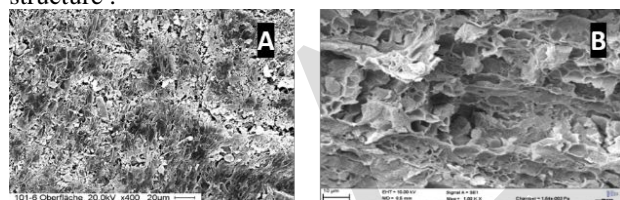
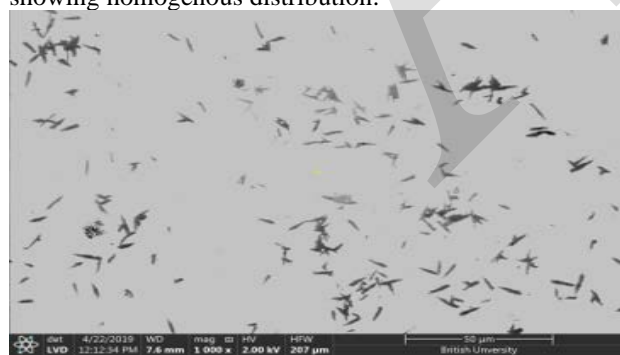


**Figure 6:** TEM image of silanized nano-hydroxyapatite showing homogenous distribution.



## DISCUSSION

In this study, photo-cured hyaluronic acid hydrogel scaffold loaded with bioactive nano-hydroxyapatite was successfully prepared using a new three component photoinitiating system based on riboflavin as a photoinitiator, DMAEMA as a coinitiator and DPIC as an accelerator. Irradiation time was 10 seconds, which is thought to be clinically acceptable. Previous studies that

used riboflavin as a photoinitiator to photo-cure hydrogels, reported an irradiation time of 40-120 seconds (9, 23).

Riboflavin (vitamin B2) was used as a natural photoinitiator with a concentration of (1% wt.). It was noticed that increasing the concentration of riboflavin above this concentration, led to no hydrogel formation upon visible light irradiation. This might be attributed to the formation of an opaque solution that hinders the irradiation light penetration as riboflavin is orange-yellow in color (24). DMAEMA was used as a coinitiator because riboflavin is a type II photoinitiator that needs an electron donor to be activated. DPIC was used as an accelerator to improve photopolymerization kinetics by reacting with inactive riboflavin radicals to produce an active radical to further initiate the polymerization reaction (25).

Methacrylated hyaluronic acid was successfully prepared with a degree of methacrylation of 36 %. This result is consistent with that of Bencherif et al., who prepared methacrylated hyaluronic acid hydrogels with degrees of methacrylation ranging from (14-90 %) and studied its influence of on the properties of prepared hydrogels. They found that a degree of methacrylation of (32%) was adequate to produce hydrogels with short irradiation time, adequate water uptake, controlled degradation and high mechanical properties (26).

Surface of nano-hydroxyapatite was modified by APTES to increase the interfacial adhesion with hyaluronic acid, to be able to produce stable hydrogels. Modification was confirmed by the FTIR spectrum which revealed the presence of APTES functional groups and TEM images showed the homogenous distribution with no agglomeration. XRD patterns, revealed three major characteristic peaks of nano-hydroxyapatite in the prepared hydrogel at  $2\Theta$  ( $31.77^\circ$ ,  $32.19^\circ$  and  $32.90^\circ$  ) which confirmed its presence in the prepared hydrogel. This finding is similar to that of Bakry et. al who distinguished nano-hydroxyapatite from brushite crystals using three major peaks (27).

In group II, it was noticed that increasing nano-hydroxyapatite concentration above ( $>0.5$  mg/ml), led to the inhibition of photo-curing of hydrogels, owing to the increased opacity of the polymer solution that hindered irradiation light penetration. The addition of nano-hydroxyapatite led to a decrease in the degree of conversion from 92 % to 51%. This can be attributed to the decrease of light penetration, owing to the increased opacity of the polymer-photoinitiating system mixture after the addition of nano-hydroxyapatite. This result is consistent with Letiune et al. who found that the addition of nano-hydroxyapatite above a certain concentration to an experimental adhesive resin decreased the degree of conversion without affecting mechanical properties (28). SEM images revealed a dense, compact and regular surface of group I. This result is in accordance with the degree of conversion results. The addition of nano-hydroxyapatite to group II led to the formation of interconnected polyhedral pores with a size of 100  $\mu\text{m}$  that mimics bone trabecular structure which is essential for angiogenesis and cell growth. This pore size is

sufficient for bone ingrowth as mentioned by Siaz et al (29).

The addition of (0.5 mg/ml) nano-hydroxyapatite to group II, increased the storage modulus by 2 folds. These results are consistent with Bouropoulos et al. who found that the addition of (0.5 % wt.) nano-hydroxyapatite to calcium alginate hydrogels increased the dynamic mechanical properties. They also found that addition of nano-hydroxyapatite above this concentration led to deterioration of mechanical properties owing to uncontrollable agglomeration of the nano-hydroxyapatite (30).

Group I showed less equilibrium swelling than group II. This result is in accordance with the SEM images which showed a dense and compact surface in group I, while in group II the interconnected porous structure led to more water uptake and swelling. This equilibrium swelling percentage is thought to be clinically acceptable because excessive swelling can lead to excessive pressure on tissues, opening of the surgical site and postoperative complications (31).

Degradation rate results showed that both hydrogels lost half of their weight after 28 days. The addition of nano-hydroxyapatite controlled the degradation rate but with an advantage of introducing a porous structure into the hydrogel which is essential for angiogenesis and bone formation. MTT assay data revealed that the cell viability % PBMCs cell lines decreased in both groups after 2 days but still remained within the range of accepted cell viability % of (>70%) according to ISO 10993-5(E) (32). Group I showed a higher cell viability % than group II. This may be attributed to the presence of APTES around the surface of nano-hydroxyapatite that led to a slight decrease in cell viability but still remained higher than the accepted range.

Histomorphometric analysis results confirmed the in vivo bioactivity of the prepared hydrogel (group II). The addition of nano-hydroxyapatite increased the osteogenic potential by one and a half folds, compared to the control group. New bone formed by creeping substitution from the adjacent original bone, filling the center of the defect. The results are in accordance with that of Nageeb et.al who confirmed the in vivo bioactivity of an injectable in-situ crosslinked hyaluronic acid hydrogel loaded with nano-hydroxyapatite in a rabbit model (22).

The null hypothesis was rejected as the addition of nano-hydroxyapatite to photo-cured hyaluronic acid hydrogels increased the mechanical properties, increased the porosity and water uptake and controlled the degradation rate. Also, the addition of nano-hydroxyapatite increased the osteogenic potential of the prepared hydrogel which proved its in vivo bioactivity.

## CONCLUSION

Injectable photo-cured hyaluronic acid hydrogel loaded with bioactive nano-hydroxyapatite was prepared using a new three component photoinitiating system composed of riboflavin, DMAEMA and DPIC. The irradiation time to form stable hydrogels was 10 seconds, which is thought to be clinically acceptable. The incorporation of

nano-hydroxyapatite led to the formation of interconnected polyhedral pores in the hydrogel, which mimics bone trabecular structure. Also, the addition of nano-hydroxyapatite increased significantly the mechanical stability by 2 folds. The prepared hydrogels were biocompatible as evident by cell viability %. In vivo bioactivity assessment revealed the osteogenic potential of the prepared hydrogel.

## Conflict of interest

The authors declare no conflicts of interest.

## REFERENCES

- Bai X, Gao M, Syed S, Zhuang J, Xu X, Zhang XQ. Bioactive hydrogels for bone regeneration. *Bioactive materials*. 2018;3(4):401-17.
- Tommasi G, Perni S, Prokopovich P. An injectable hydrogel as bone graft material with added antimicrobial properties. *Tissue engineering Part A*. 2016;22(11-12):862-72.
- Kogan G, Soltes L, Stern R, Gemeiner P. Hyaluronic acid: a natural biopolymer with a broad range of biomedical and industrial applications. *Biotechnology letters*. 2007;29(1):17-25.
- Bae MS, Ko NR, Lee SJ, Lee JB, Heo DN, Byun W, et al. Development of novel photopolymerizable hyaluronic acid/heparin-based hydrogel scaffolds with a controlled release of growth factors for enhanced bone regeneration. *Macromol Res*. 2016;24(9):829-37.
- Kattimani VS, Kondaka S, Lingamaneni KP. Hydroxyapatite-Past, Present, and Future in bone regeneration. *Bone Tissue Regener Insights*. 2016;7:9-19.
- Huang R, Choe E, Min D. Kinetics for singlet oxygen formation by riboflavin photosensitization and the reaction between riboflavin and singlet oxygen. *J Food Sci* 2004;69:726-32.
- Baier LJ, Bivens KA, Patrick CW, Schmidt C. Photocrosslinked hyaluronic acid hydrogels: natural, biodegradable tissue engineering scaffolds. *Biotechnol Bioeng*. 2003;82(5):578-89.
- Tavsanli B, Okay O. Mechanically strong hyaluronic acid hydrogels with an interpenetrating network structure. *Eur Polym J*. 2017;94:185-95.
- Park H, Choi B, Hu J, Lee M. Injectable chitosan hyaluronic acid hydrogels for cartilage tissue engineering. *Acta biomaterialia*. 2013;9(1):4779-86.
- Michael FM, Ratnam CT, Khalid M, Ramarad S, Walvekar R. Surface modification of nanohydroxyapatite and its loading effect on polylactic acid properties for load bearing implants. *Polym Compos*. 2018;39(8):2880-8.
- Kamoun EA, Abu-Saied MA, Doma AS, Menzel H, Chen X. Influence of degree of substitution and folic acid coinitiator on pullulan-HEMA hydrogel properties crosslinked under visible-light initiating system. *Int J Biol Macromol*. 2018;116:1175-85.
- Hashemi DA, Mirzadeh H, Samadi N, Bagheri-Khoulenjani S, Atai M, Imani M. Potential Application of a Visible Light-Induced Photocured Hydrogel Film as a Wound Dressing Material. *J polym* 2015;2015:1-10.

13. Uswatta SP, Okeke IU, Jayasuriya AC. Injectable porous nano-hydroxyapatite/chitosan/tripolyphosphate scaffolds with improved compressive strength for bone regeneration. *Materials science & engineering C, Materials for biological applications*. 2016;69:505-12.
14. Mondal S, Hoang G, Manivasagan P, Moorthy MS, Nguyen TP, Vy Phan TT, et al. Nano-hydroxyapatite bioactive glass composite scaffold with enhanced mechanical and biological performance for tissue engineering application. *Ceramics International*. 2018;44(13):15735-46.
15. O'Connell CD, Zhang B, Onofrillo C, Duchi S, Blanchard R, Quigley A, et al. Tailoring the mechanical properties of gelatin methacryloyl hydrogels through manipulation of the photocrosslinking conditions. *Soft matter*. 2018;14(11):2142-51.
16. Kamoun EA, H. M. Crosslinking behavior of dextran modified with hydroxyethyl methacrylate upon irradiation with visible light-Effect of concentration, coinitiator type, and solvent. *J Appl Polym Sci*. 2010;117(6):3128-38.
17. Patterson J, Siew R, Herring SW, Lin AS, Guldberg R, Stayton PS. Hyaluronic acid hydrogels with controlled degradation properties for oriented bone regeneration. *Biomaterials*. 2010;31(26):6772-81.
18. Almahdy O, ElFakharany EM , ElDabaa E, Ng TB, Redwan E. Examination of the activity of camel milk casein against hepatitis C virus (genotype-4a) and its apoptotic potential in hepatoma and hela cell lines. *Hepat Mon*. 2011;11(9):724-30.
19. Tyliszczak B, Drabczyk A, Kudłacik-Kramarczyk S, Bialik-Wąs K, Sobczak-Kupiec A. In vitro cytotoxicity of hydrogels based on chitosan and modified with gold nanoparticles. *J Polym Res*. 2017;24:1-7.
20. Haridas N, Rosemary MJ. Effect of steam sterilization and biocompatibility studies of hyaluronic acid hydrogel for viscosupplementation. *PolymDegrad and Stab*. 2019;163:220-7.
21. Mostafa D, Aboushelib M. Bioactive-hybrid-zirconia implant surface for enhancing osseointegration: an in vivo study. *International journal of implant dentistry*. 2018;4(1):1-7.
22. Nageeb M, Nouh SR, Bergman K, Nagy NB, Khamis D, Kisiel M, et al. Bone Engineering by Biomimetic Injectable Hydrogel. *Molecular Crystals and Liquid Crystals*. 2012;555(1):177-88.
23. Chichiricco P, M., Riva R, Thomassin J, M., Lesoeur J, Struillou X, Le Visage C, et al. In situ photochemical crosslinking of hydrogel membrane for Guided Tissue Regeneration. *Dent Mater*. 2018;34(12):1769-82.
24. Kim S, Chu C. Visible light induced dextran-methacrylate hydrogel formation using (-)-riboflavin vitamin B2 as a photoinitiator and L-arginine as a co-initiator. *Fibers and Polymers*. 2009;10(1):14-20.
25. Kim D, Scranton A. The role of diphenyl iodonium salt (DPI) in three-component photoinitiator systems containing methylene blue (MB) and an electron donor. *J Polym sci A Pol chem*. 2004;42(23):5863-71.
26. Bencherif SA, Srinivasan A, Horkay F, Hollinger JO, Matyjaszewski K, Washburn NR. Influence of the degree of methacrylation on hyaluronic acid hydrogels properties. *Biomaterials*. 2008;29(12):1739-49.
27. Bakry AS, Takahashi H, Otsuki M, Tagami J. Evaluation of new treatment for incipient enamel demineralization using 45S5 bioglass. *Dent Mater*. 2014;30(3):314-20.
28. Leitune VCB, Collares FM, Trommer RM, Andrioli DG, Bergmann CP, Samuel SMW. The addition of nanostructured hydroxyapatite to an experimental adhesive resin. *J Dent* 2013;41(4):321-7.
29. Saiz E, Gremillard L, Menendez G, Miranda P, Gryn K, Tomsia AP. Preparation of porous hydroxyapatite scaffolds. *Materials Science and Engineering: C*. 2007;27(3):546-50.
30. Bouropoulos N, Stampolakis A, Mouzakis DE. Dynamic Mechanical Properties of Calcium Alginate-Hydroxyapatite Nanocomposite Hydrogels. *Sci Adv Mat* 2010;2(2):239-42.
31. Fricain JC, Granja PL, Barbosa MA, De Jeso B, Barthe N, Baquey C. Cellulose phosphates as biomaterials. In vivo biocompatibility studies. *Biomat*. 2002;23(4):971-80.
32. ISO. International Organization of Standardization .ISO 10993-5:2009(E)-Biological evaluation of medical devices-Part 5:Tests for in vitro cytotoxicity. ISO 2009;ISO 10993-5:2009 (E).